Aerodynamic Design Space Exploration of a Fuselage Boundary Layer Ingesting Aircraft

van Sluis, M.; della Corte, B.; Gangoli Rao, A.

DOI
10.2514/6.2023-4069

Publication date
2023

Document Version
Final published version

Published in
AIAA AVIATION 2023 Forum

AIAA AVIATION Forum
12-16 June 2023, San Diego, CA and Online
AIAA AVIATION 2023 Forum

10.2514/6.2023-4069

Aerodynamic Design Space Exploration of a Fuselage Boundary Layer Ingesting Aircraft

M. van Sluis * , B. DellaCorte † and A. Gangoli Rao ‡

Fuselage Boundary-Layer Ingestion (BLI) is a promising example of synergistic design and propulsion-airframe integration to reduce fuel burn. For a BLI configuration, the aero-propulsive performance of the aircraft is a result of the complex aerodynamic interaction between the fuselage airframe and the BLI propulsor. This paper presents a design method for the aft fuselage including the propulsor shrouding to minimize the required shaft power of an aft-mounted propulsor in the conceptual design phase. First, a global aerodynamic design space exploration is carried out using Computational Fluid Dynamics (CFD) to identify the key design parameters and their influence to the aerodynamic performance of the propulsive fuselage. An optimization study is subsequently carried out to improve the aerodynamic performance of a baseline design. The optimization was performed for a turbo-electric BLI configuration and within representative design constraints. The optimization achieved a decrease of approximately 10% **of the isentropic shaft power required for the aft-mounted propulsor for a constant net force acting on the propulsive fuselage. The presented methodology and the resulting design practices can be effectively applied to other advanced aircraft configurations.**

I. Introduction

To make future civil aviation sustainable, ambitious goals regarding emissions and noise have been set by the Advisory Council for Aeronautics Research in Europe (ACARE), described in the FlightPath 2050 [1]. These goals, as part of the Strategic Research and Innovation Agenda (SRIA) [2], aim at a reduction of 60% CO2 emission per passenger kilometre by 2035 relative to the year 2000. Evolution of current aircraft technology will fall short of these ambitions. A step-change in aircraft technology and design is required in order to meet the goals. Many different novel technologies are being investigated, such as full laminar flow wings [3] and hybrid electric propulsion [4]. However, in order to meet the emission targets for aviation, a multitude of novel technologies will have to be integrated in a synergistic manner, as no single technology in existence today appears to be able to fulfil the requirements alone. Boundary Layer Ingestion (BLI) is one such technology to reduce aircraft fuel burn by exploiting synergistic airframe-propulsion integration. In a BLI configuration, the propulsor is tightly integrated onto the airframe and operates on the boundary-layer flow. As a

*Researcher, Flight Performance and Propulsion, Delft University of Technology, M.vansluis@tudelft.nl
†PhD candidate, Flight Performance and Propulsion, Delft University of Technology, B.DellaCorte@tudelft.nl
‡Associate professor, Flight Performance and Propulsion, A.GangoliRao@tudelft.nl

consequence, the BLI propulsor re-cuperates the momentum and energy deficit in the boundary layer, thereby reducing the viscous dissipation in the wake [5] [6]. A conceptual-level study has shown that ingestion of the full fuselage boundary layer by a single circumferential propulsor yields the largest potential aerodynamic saving [7]. In particular, it was found that such a configuration, named the Propulsive Fuselage Concept (PFC), using a gas-turbine driven BLI propulsor, could achieve a net fuel burn reduction of approximately 10% compared to a conventional baseline configuration [8]. A similar order of magnitude fuel burn reduction was found by more recent NASA studies on the turbo-electric NASA STARC-ABL aircraft [9] [10]. In order to improve the aerodynamic benefit of the fuselage annular (or Type II) boundary layer ingestion, aerodynamic shape optimization of both the fuselage and its corresponding nacelle and boat tail is required. Differently from a conventional aircraft design, the objective function for the optimization process of a tightly coupled BLI system does not necessarily have to be drag minimization. The tight coupling of the propulsor and the airframe requires a novel design approach where the combined performance of the system should be considered as a whole.

Recent studies attempt to optimize the fuselage and aft nacelle geometry to improve the different aspects of the aircraft performance. For example, the fuselage-fan inlet distortions, induced by the wings and fuselage upsweep in the STARC-ABL concept, were minimized through CFD-based shape optimization of the shroud and hub contours [11]. The adjoint-based shape optimization yielded to noticeable lower distortion levels while the drag increase was constrained to a single drag count. However, the improvements in the distortion levels were accompanied by modest increases in the required power of the propulsor to match the thrust requirement. In a similar computational approach [10], it was attempted to improve the aerodynamic propulsive efficiency by altering the shaping of the nacelle and aft fuselage contour. Free-Form Deformation (FFD) was applied to the entire aft fuselage section, while a turbofan model was implemented to emulate the BLI fan. The main finding of the work [10] is that, depending on the transmission efficiency of the electrical power system, the propulsor size is altered to maximize the Power Saving Coefficient (PSC). Although the propulsor size was clearly the dominant factor, the contour shaping of the fuselage and nacelle were also altered during the optimization to improve the inflow to the propulsor. However, the paper is focussed on the PSC of the final optimized configuration and does not distinguish between the various contributions of the design parameters. Although adjoint aerodynamic shape optimization has shown to improve the performance of BLI aircraft designs [12], it does not give a comprehensive insight into the various interactions of the individual components. In order to streamline the conceptual design phase of a BLI configuration, it would be very useful to have a qualitative and quantitative understanding of the design parameters. In a different study [13], the aft geometry on the STARC-ABL concept was optimized using OpenVSP [14]. Rather than using mathematical control points to describe the geometry, design criteria such as ellipse radius and tangent angles were prescribed. The geometry was optimized for various levels of FPR and net force coefficient, thereby minimizing the shaft power. Although the work [13] discusses the performance of the optimized designs in detail, little insight is provided regarding which geometric parameters have a higher influence the aerodynamic performance of a

fuselage BLI configuration. In another work [15], the duct and shrouding of a regional electric aircraft is optimized, using a parametrized representation of the nacelle and duct shaping. The optimization is performed for three different objective functions, namely maximum thrust, lowest flow mechanical power and maximum propulsive efficiency. Each objective yields a noticeably different geometry. However, only two parameters describing the inlet lip of the duct are included in the actual analysis, limiting the explored design space. As the paper focusses on multidisciplinary design of the particular aircraft, the specific knowledge gained in terms of aft-body shaping for a BLI configuration is limited.

In this paper, a systematic approach for the aerodynamic design space exploration and optimization of a (axisymmetric) bare PFC configuration (i.e.fuselage including BLI propulsive device) is described. The aerodynamic analysis was based on RANS CFD simulations and a body-force model for the fuselage propulsor. A comprehensive set of geometrical and operational parameters were considered to accurately and flexibly describe the PFC geometry and flow conditions. A sub-set of the most influencing parameters was obtained through a Design Space Exploration (DSE), after which a global optimization was performed to minimize the fuselage-fan isentropic power. The goal of the paper is to demonstrate which are the important sensible parameters driving the propulsive fuselage design in the conceptual design phase of the PFC. The methodology described in the present work has been used for aircraft level optimality studies, as described in [37].

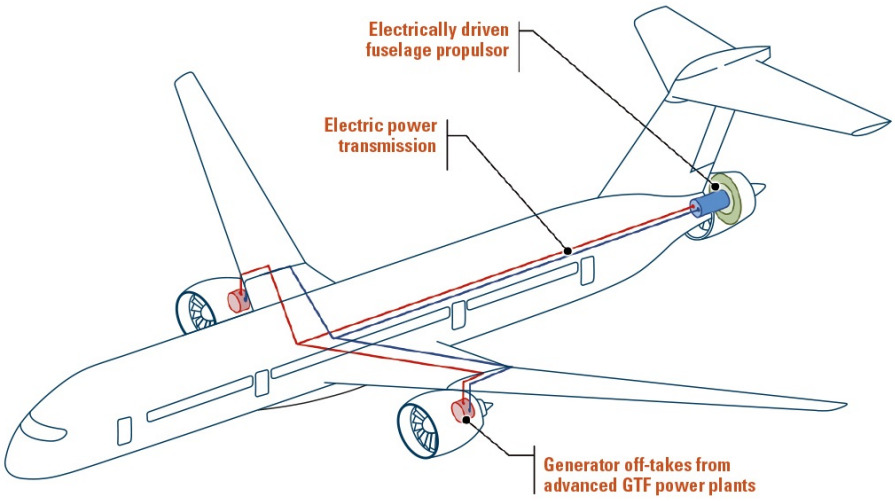

Fig. 1 Overview of aircraft layout and turbo-electric drivetrain (image: Bauhaus Luftfahrt)

A. Background

The aerodynamic design space exploration in this work is conducted for the PFC within the CENTRELINE project [16][17]. The design is focussed on an Airbus A330-300 class aircraft with an entry to service in 2035. The aircraft is being designed to carry 340 passengers over a range of 6500 nm. A turbo-electric drive-train is utilized, with power

off-take from the under-the-wing Geared Turbo-Fan (GTF) engines to supply an electric motor driving the BLI fan in the rear of the aircraft. The electric motor is rated for 8 MW design power and 95% efficiency. The FF is aimed to be able to provide 6% thrust at top-of-climb [18]. The main level requirements are listed in Table 1. A schematic of the concept is shown in Figure 1.

Table 1 Overview of CENTRELINE top-level requirements [18]

Parameter	Requirement
Range	6500 nmi
Passengers	340
Design cruise Mach	0.82
Cruise altitude	FL350
Maximum cruise altitude	FL410
Approach speed	140KCAS

II. Methodology

In order to conduct a thorough aerodynamics design space exploration, the design space needs to be well defined. The definition of the aerodynamic design space is important to ensure that no parts of the design space are excluded from the exploration. In general, one could divide the aerodynamic design space into two categories, as depicted in Figure 2, namely *operational* and *geometric* design parameters. The geometric parameters of the PFC can be divided into aircraft level and component level parameters. In case of the PFC, the Fuselage Slenderness Ratio (FSR) and the duct height of the Fuselage Fan (FF) are examples of aircraft level parameters. These parameters directly define the overall geometric shape of the aircraft. The same hold true for the operational parameters, which can be either dictated by the mission design or the system performance.

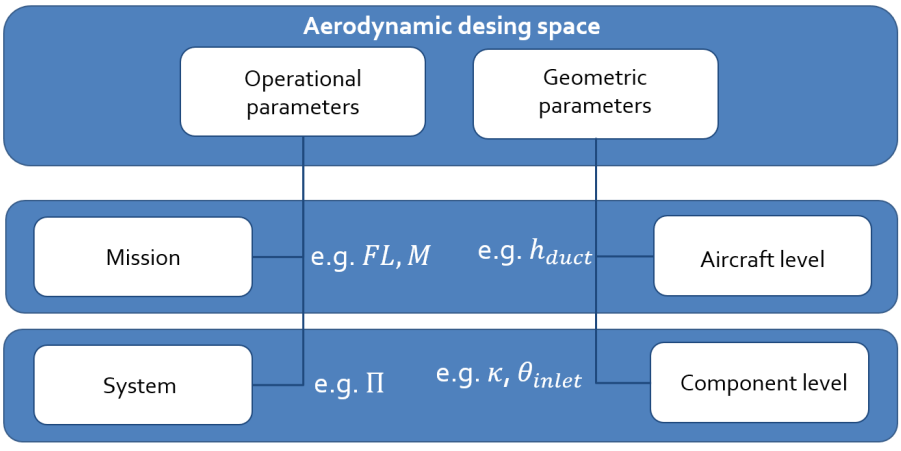

Fig. 2 Classification of the aerodynamic design space parameters

A MATLAB®-based framework has been set-up to analyse a very large number of PFC geometries. An overview of

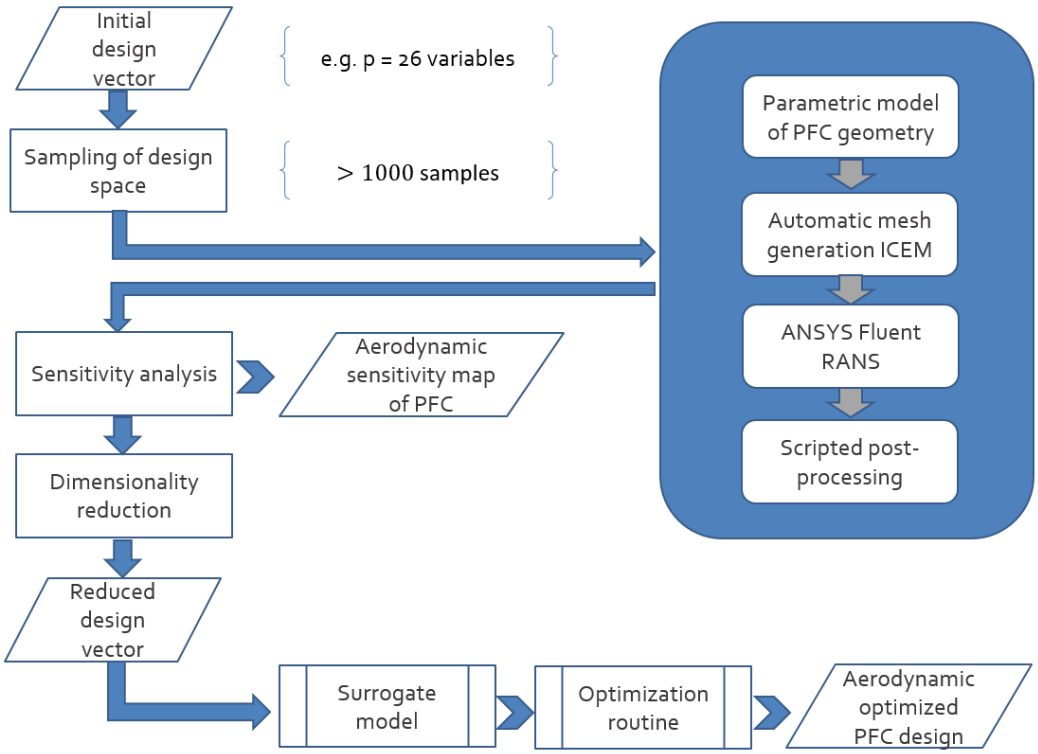

Fig. 3 Flow diagram of the aerodynamic design space exploration procedure

the workflow is presented in Figure 3. The principal step is to generate a parametric model of the PFC. The main requirements is that the model should be flexible enough to allow for a wide variety of fuselage and nacelle shapes, in order to have minimum restrictions of the design space. Next, the design space is surveyed using statistical methods for quasi-random sampling. Each sample reflects a unique geometry and operating condition. The sample space is consecutively fed into the main computational framework, where the design vector is translated into a geometry and a mesh. A mesh quality above a specified threshold was ensured to provide consistent and accurate results. Subsequently the Reynolds Averaged Navier-Stokes (RANS) analysis was carried out using ANSYS® Fluent 18.2 and the subsequent results were post-processed by a scripted routine. Based on the solution data of evaluated samples, a sensitivity study is carried out to identify the driving parameters. Using the knowledge from the sensitivity analysis, a surrogate model of the aerodynamic response can be constructed and be used in an optimization routine.

A. Parametrization of the Propulsive Fuselage Concept

In order to describe the bare PFC geometry by a limited set of design parameters, a parametric model of the geometry has been developed. The parametrization of the geometry needs to be as flexible as possible, to be able to generate a wide variety of geometries. At the same time, it should be ensured that the geometries created by the parametric model are feasible and do not violate the basic constraints set beforehand. In order to combine these two op-

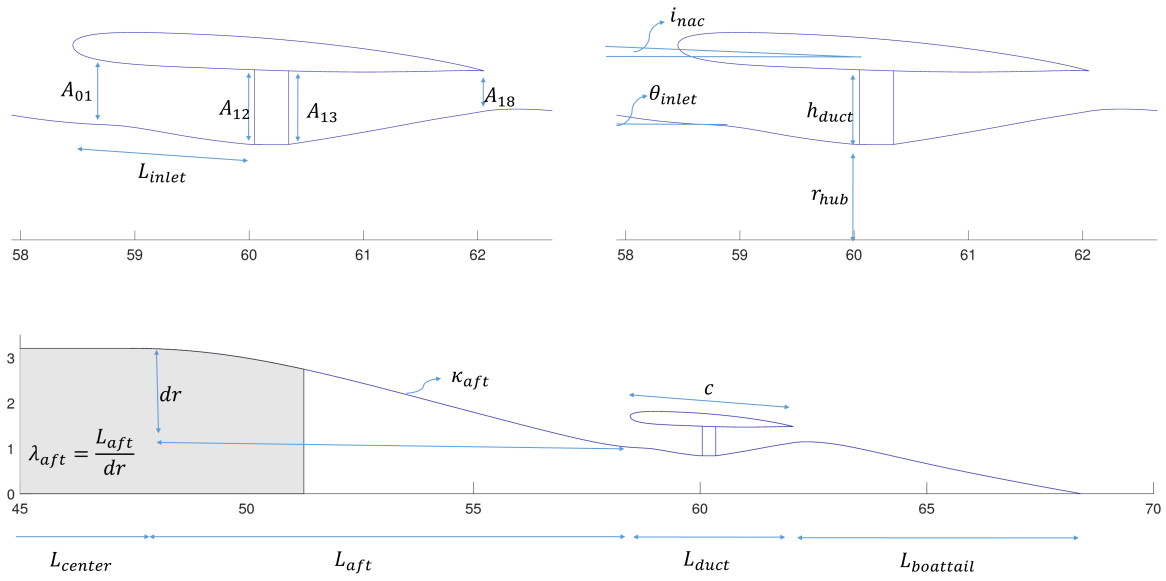

Fig. 4 Drawing with main length parameters of an example PFC fuselage geometry as described by the parametric model. Note that the cabin area is indictated by the hilighted area.

posing requirements, a parametric model has been developed that incorporates both flexibility and basic engineering rules.

Since the aft-fuselage is the main area of interest of the PFC, the parametric model is focussed on the aft section of the fuselage. Therefore it does not include the wings, empennage or main under-wing podded engines. A conventional fore-body shape is adopted from the Engineering Sciences Data Unit (ESDU) (fore-body 9 [19]). The slenderness of the nose section is kept constant, to ensure shape similarity with varying fuselage diameter. A second requirement for the PFC fuselage is that the effective floor area is kept constant, in order to compare the performance of the PFC to the R2035 reference aircraft [20]. Since a study into the cabin topology is beyond the scope of the current work, a minimal fuselage diameter was set to bound the useable floor area. For sizing of the main fuselage dimensions, the fuselage diameter is given as primary input, together with the slenderness ratio of the aft fuselage section up to highlight of the duct. An iteration loop is used to find the corresponding length of the fuselage centre section. Since the relative axial position of the FF is an important design parameter and the lengths of the upstream section are already determined, the length of the boat tail is derived from the total fuselage length. The position of the FF is used as the reference location for the aft geometry. An overview of the main fuselage dimensions is shown in Figure 4.

The curves of the fuselage geometry are constructed using Non-Uniform Rational B-Splines (NURBS) [21]. Widely used in CAD modelling, NURBS enable to make localized changes to the geometry without affecting the overall shape of the curve. This in an important property as it allows to study individual changes to geometry rather than

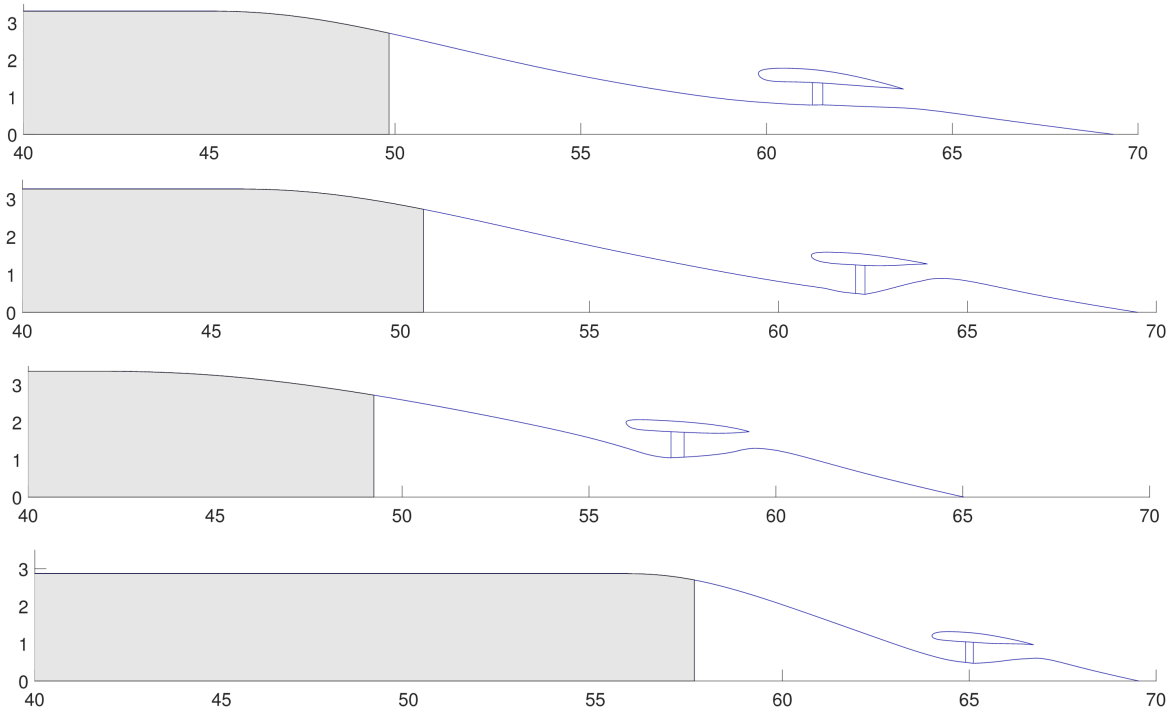

Fig. 5 Examples of aft-fuselage geometries initiated by the parametric mode using random design parameter samples. Dimensions are given in meters.

combined effects. First order continuity is enforced between the NURBS segments, to ensure a curvature continuity. Since the aim of the work is to gain an understanding of the aerodynamic behaviour of the design, the control points of the NURBS are either related to a design parameter or embedded engineering rules. As such, there are no 'free floating' control points in the design vector. The nacelle geometry was treated in a similar manner, albeit not with NURBS. Instead, it was chosen to use a third order Bezier-Parsec approach [22], which was developed to describe airfoils using design parameters only. In total, 12 design variables are used to describe the airfoil geometry. The flow channel to the fuselage fan is dictated by the nacelle, whose chord length is a function of the diameter of the FF. The positioning of the nacelle is performed with the FF location as a reference. The length of the inlet and the incidence angle of the nacelle are both determined with respect to the FF. To promote a feasible duct geometry, the cross-section area of the throat and the duct exit are prescribed as a function of the FF inlet face area.

The flexibility of the parametric model is shown in Figure 5, where a few examples of generated PFC designs are shown for a set of (bounded) random design parameters. As can be observed, the model is able to produce substantially different PFC designs. In order to ensure that the resulting designs from a random combination of the in total 26 design variables are feasible designs, the bounds were chosen carefully. For example, the bounds for the nacelle are set such that the 3rd order Bezier-Parsec (BP3333)[22] parametrization always yields a feasible airfoil representation.

Table 2 Overview of the design parameters and their respective bounds

Parameter	x_{min}	x_{max}	unit
D_{fus}	5.50	6.90	m
κ_{aft}	0.40	1.50	-
λ_{aft}	3.5	8.00	-
x_{FF}	0.84	0.905	-
l_{inlet}/c	0.25	0.50	-
h_{duct}	0.30	1.00	m
r_{hub}/r_{tip}	0.369	0.625	-
θ_{inlet}	0.0	20.0	deg
c/D_{FF}	0.80	1.40	-
$(t/c)_{max}$	0.08	0.11	-
ϱ_{LE}	-0.50	-0.10	-
γ_{LE}	10	30	deg
x_c/c	0.30	0.50	-

Parameter	x_{min}	x_{max}	unit
y_c/c	-0.02	0.05	-
κ_c	-1.00	-0.10	-
x_t/c	0.25	0.40	-
κ_t	-0.08	-0.01	-
δ_{TE}	8.0	12.0	deg
β_{TE}	5.0	12.0	deg
i_{nac}	0.0	8.0	deg
A_1/A_{12}	0.90	1.05	-
A_{13}/A_{12}	0.95	1.00	-
A_{18}/A_{12}	0.60	0.70	-
Π	1.20	1.50	-
FL	310	390	100ft
M	0.75	0.85	-

Furthermore, it is made sure that no excessive long or short aft-fuselage section are created. Nevertheless, for some specific combinations of parameters a non-feasible geometric design can still occur. These geometries are filtered out by a set of engineering constraints, such as bounds on boat-tail cone angles, and are not included in the analysis.

B. Sampling of aerodynamic design space

In order to cover as much of the design space as possible, a suitable sampling strategy should be adopted. Ideally, one would use permutations of all possible combinations of design parameters to ensure complete sampling of the design space. However, such an approach is only feasible when the number of design variables is very small or the computational cost of analysis is low. For the current application, a quasi-random sampling approach is better suited. Many different algorithms and methods are in existence [23], such as the Latin Hypercube Sampling (LHS) method. A multitude of different LHS derived methods exist today, each method trying to increase the space-filling capability of the sampling and reducing the correlation between individual samples. For the current work, a novel method combining both Latin Hypercube design and stratification [24] is selected. The partial stratification of the variables allows one to group design variables which are expected to have a strong correlation. For example, it is expected that the FPR and duct height h_{duct} will have a strong coupling on the required shaft power by the FF. Grouping the parameters together will ensure the optimal spacing of the samples in the design space with respect to each other. In case the anticipated interaction is not present, the quality of the sampling would not be penalized. A three-fold stratification plan was used, meaning that groups of three design parameters were made for stratification, prior to the hypercube sampling. In total 9261 samples were generated and used as input for the analysis framework.

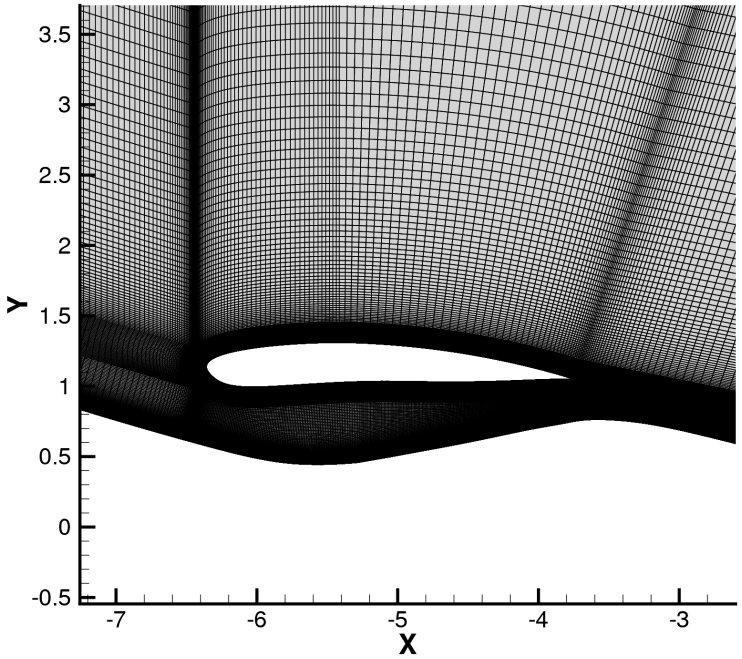

Fig. 6 Example of a mesh, generated by the framework, for an arbitrary sample PFC geometry. Coordinates are in meters and measured from the trailing edge

C. Grid generation

To prepare the generated bare PFC geometries for analysis, a Matlab® routine has been developed that generates the topology of the mesh and writes the required input files for Ansys®ICEM. The latter program is used for the computation of the actual mesh. For the core of the Matlab tool to prepare the geometry, modified open-source Matlab® routines [25] have been used. A structured C-grid is created for the main domain and two embedded O-grids wrap the fuselage body and the FF nacelle. Since the turbulence will be resolved up to the wall, the mesh complies with the $Y^+ \leq 1$ requirement. The latter is crucial to capture the development of the boundary layer in the best possible way using RANS models. In total, a typical 2D axis-symmetric mesh contains about $360,000$ to $400,000$ cells. For every generated mesh, the mesh quality statistics were analysed automatically by ANSYS® ICEM to assess the mesh quality. The quality criterion used in ICEM is a weighted combination of cell warpage, orthogonal quality and the determinant. The statistical mesh properties are shown in Table 3. As can be observed, the average of the minimum and mean quality index of the mesh are high. However, the standard deviation of the average minimum quality index is relatively high as well, indicating a wider variation in cell quality. Due to an imperfect conversion in the interface between Matlab® and ICEM, the total success rate of the mesh routine was approximately 51%

III. Setup of CFD simulation

The computational analysis of the flow field using RANS was carried out using the commercial software ANSYS® Fluent (version 18.2). The pressure-coupled, axis-symmetric solver was used. The fluid was modelled as an ideal

Table 3 Statistics of mesh quality criterion by ICEM for meshes of converged simulations (N = 3560). The quality index for hexa elements is a weighted diagnostic between the determinant, orthogonal quality and cell warpage.

Quality Index	$\bar{x}$	σ
Minimum quality	0.8915	0.1486
Average quality	0.9883	0.0146

compressible gas, with the fluid viscosity being modelled by the three-coefficient method of Sutherland [26]. Since the flow is assumed compressible, the energy equation is enabled. Turbulence is modelled by the $k-\omega$ Shear Stress Transport (SST) developed by Menter [27]. Compressibility corrections and Kato-Launder production limiter were enabled. Spatial discretization of the turbulence transport equation was done through a second-order accurate scheme (QUICK) [28]. The discretization of the momentum and energy equation are in turn taken care of by a third-order MUSCL [29] scheme.

A. Fan modelling

An important aspect for the analysis of the PFC is the modelling of the fuselage fan in CFD. A through-flow nacelle approach (i.e.no inflow or outflow domain boundaries) was used to preserve the boundary layer over the fan stage. In order to accomplish this, a simple body-force was developed and implemented using a User-defined Function (UDF). In the mesh, a separate fluid domain is defined which represent the box volume around the fan. The UDF adds an axial momentum density S_m (N/m^3) source term to all cells within the domain containing the fan. Note that momentum is only added in axial direction, assuming zero swirl or radial changes in momentum. This is acceptable as the stator vanes behind a fan should recover most of the swirl [30]. Shown in Figure 7 is the change in total momentum mass-averaged over the duct area. The volume of the FF is hi-lighted in grey. As can be seen, the axial velocity is decreased over the fan, whereas the static pressure is increased. Since the fluid is assumed to be compressible, additional source terms for the energy equation S_e are added. The energy is computed as the local work done by the external force of the momentum density source. As such, the total enthalpy of the fluid is increased as shown in Figure 8. Since the fan total pressure ratio is the main design parameter for the FF, the momentum source term is adjusted iteratively by the UDF until the mass-averaged FPR is equal to the specified target fan pressure ratio.

B. Drag-thrust bookkeeping

As a results of the high level of integration of the aft-mounted BLI propulsor, the conventional thrust-drag bookkeeping schemes are not suitable as the distinction between the propulsor and the airframe is ambiguous. However, a distinction between thrust and drag is desired from an aircraft conceptual design point-of-view. The simple fan model, as described

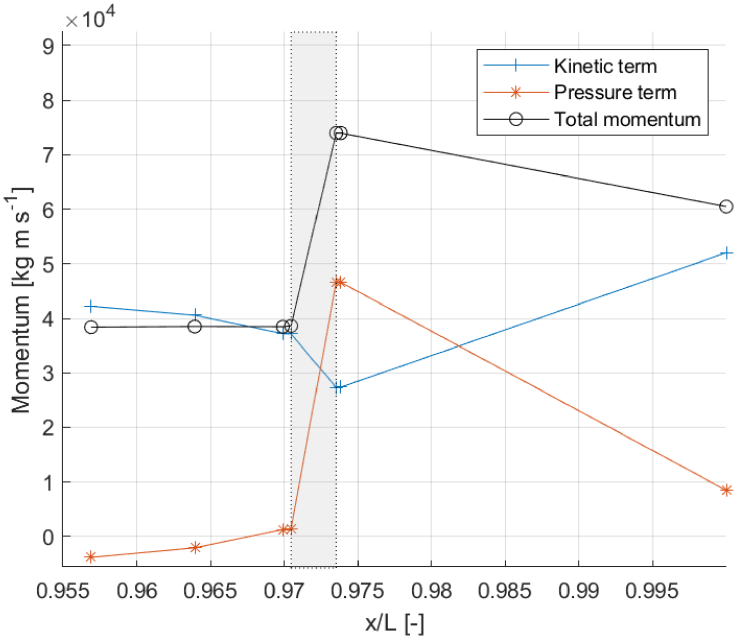

Fig. 7 Example of mass-averaged total momentum across the duct using the body force model.

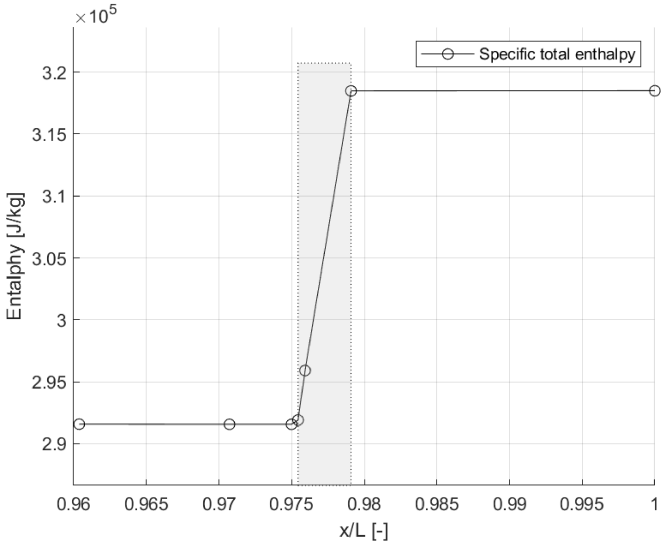

Fig. 8 Example of mass-averaged specific total enthalpy across the duct using the body force model.

in III.A, allows for a clear definition of the propulsive force by the actuator volume and drag. Integration of the momentum density source term (N/m^3) over the volume defining the FF directly yields the propulsive force. Note that the propulsive force by the actuator volume is (by definition) not identical to the FF thrust [31]. The drag is obtained by integration of the viscous and pressure normal forces over all the solid surfaces. As such, the force balance of the bare PFC can be reduced to:

$$F_{\text{NPF,bare}} = F_{\text{T,FF}} - D_{\text{bare}} = \iiint_V S_a \, dV - \iint_S \tau \, dS - \iint_S p \cdot \hat{n} \, dS \tag{1}$$

All quantities in the above equation are available in the numerical results. Similarly, the energy provided by the FF to the flow can be computed as:

$$P_{\text{shaft, id}} = \iiint_V S_e \, dV \tag{2}$$

Note that the integrated energy source terms yields the required power by the FF without including any losses. The efficiency of the fan is explicitly not included to reduce complexity and avoid additional assumptions. As such, $P_{\text{shaft,id}}$ represents the minimum required power. Since NPF and ideal shaft power are dimensional quantities, a non-dimensional term called the BLI efficiency factor has been defined:

$$f_{\eta,\text{PFC,bare}} = \frac{F_{\text{NPF, bare}} \cdot V_\infty}{P_{\text{shaft,id}}} \tag{3}$$

The above equation expresses the ratio between the rate of work done by the NPF acting on the bare PFC and the ideal shaft power. Although the relation is very straightforward, it allows to directly asses the performance different PFC design. Since the relation is easy to evaluate and is sensitive to even small design changes, it is well suited to be used in the design space exploration.

IV. Results

With the computational framework in place, the aerodynamic design space exploration was carried out. The analysis has two objectives: first it is attempted to obtain insight in the sensitivity of the various design parameters on the aerodynamic performance of the PFC. The second objective is to use the knowledge gained from the design space exploration to optimize the axisymmetric bare PFC design.

A. Sensitivity analysis

The main aim of the aerodynamic design space exploration is to gain an understanding of how each of the design parameters is influencing the aerodynamic performance of the PFC. Ideally, one would look at both the influence of the

isolated design parameters as well as their combined effect on the aerodynamic performance. Statistical methods, such as Principal Component Analysis (PCA) [32], can be used to determine the driving parameters in large design problems with computational expensive analysis [33]. Such a statistical insight into the design parameter dependency is desired. However, no convergence of the PCA result was obtained for the current dataset, as there remained a dependency on the number of included results. The sensitivity of the various design parameters is found to be different in orders of magnitude. It is believed that this, together with the interdependency of the parameters, caused too much scattering of the gradient data.

Nonetheless, to still be able to understand the main sensitivities of the aerodynamic design for the PFC, a one-dimensional sensitivity study has been carried out. An initial design, representing the mean of the design vector, has been selected as a baseline. Each design parameter was changed, one by one, within their respective limits. Results for the most dominant design parameters with respect to $f_{\eta,\text{PFC,bare}}$ of the baseline design are shown in Figure 9. The data points are fitted with a second order polynomial function. As can be observed, the FPR together with the height of the FF duct appear to be the dominant design parameters for the aerodynamic performance of the PFC. This is to be expected, as together these parameters dictate the required idealized power by the FF. Despite this, a few interesting observations can still be made. First, it can be seen that for the baseline design, increasing the FPR is beneficial but the benefit is diminishing towards the upper bounds of the FPR. On the other hand, the performance of the bare PFC is reducing rapidly when the FPR is lowered. It should be noted that the geometry is not adapted with any change in design FPR. Therefore, the area ratio of the duct inlet and exit are not adjusted to minimize spillage drag and facilitate optimal mass-flow. Nevertheless, it does show that the drag penalty due to addition of the FF nacelle can be offset most by increasing the propulsive force of the FF as much as possible. A similar observation can be made for the duct height. For higher duct heights, the additional momentum deficit that is ingested by the fan is diminishing. Furthermore, the nacelle is no longer embedded in the lower total pressure region of the boundary layer, thereby increasing its drag. The next set of design parameters that play an important role, are the Mach number and the area ratio of the duct exit. Both effectively determine the magnitude of the mass flow through the duct, which is again driving the power requirement of the fan.

The shaping of the rear fuselage section upstream of the FF appears to be of lesser importance, based on the sensitivities of λ_{aft} and κ_{aft}. Nevertheless, a trend can be observed which suggest that for the baseline design, a shorter rear section with a more convex aft body shape would be beneficial. In terms of fuselage diameter, the trend suggests a slightly lower fuselage diameter, which would result into a longer fuselage centre section. Also shown in Figure 9 is the relative axial position of the FF, which is favoured to be positioned at the aft. However, as one can see from the last data point, there appears to be a drop towards the upper bounds. This could be explained by the fact that the length of the boat tail is reduced if the FF is positioned further aft. The pressure forces acting on the boat tail have a force component in flight direction, reducing the drag. Shortening of the boat tail

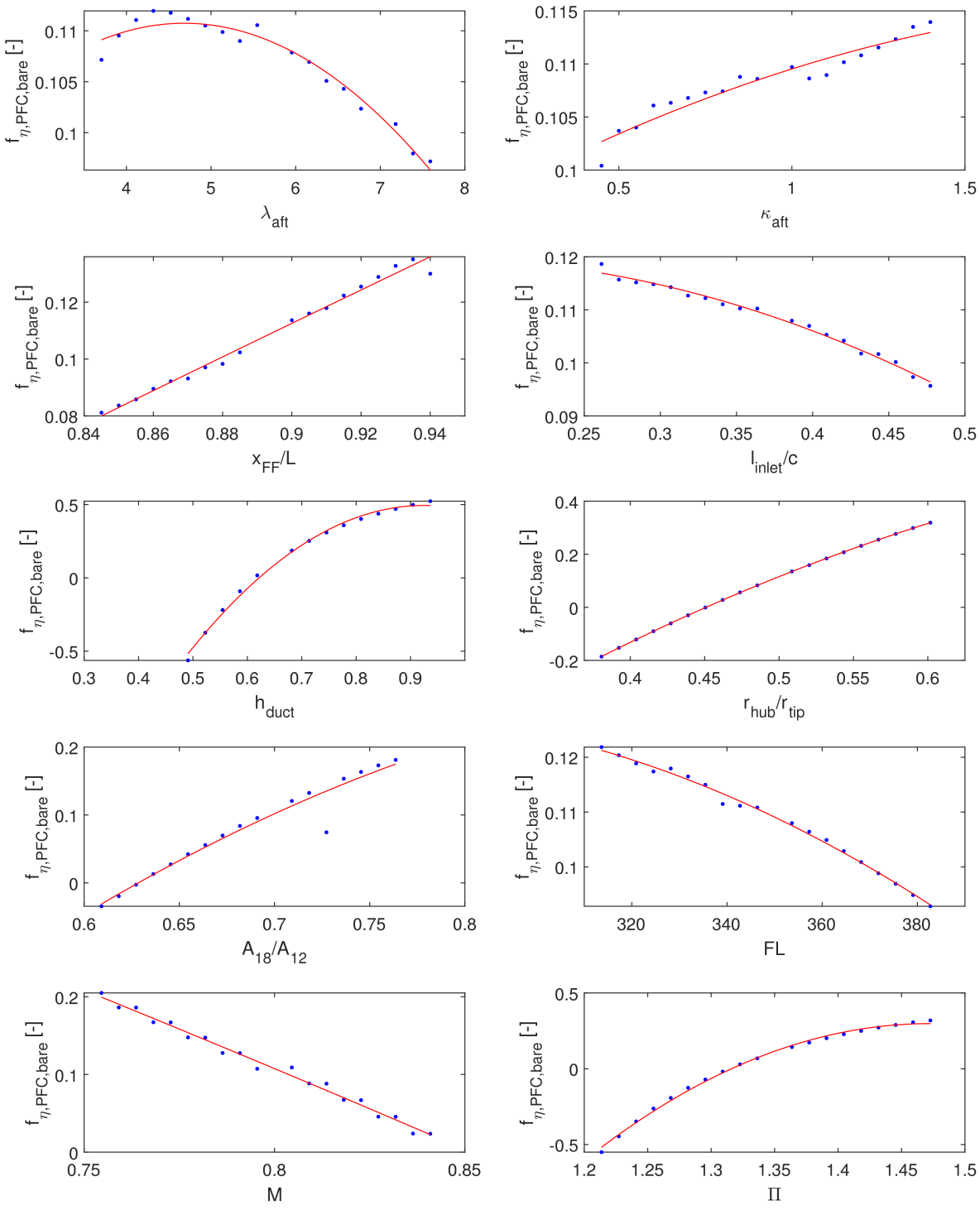

Fig. 9 Plots of 1-dimensional sensitivity of the design parameter w.r.t to the boundary layer ingestion efficiency factor in comparison with the baseline design. All other parameters are kept constant

reduces the exposed surface area and with that decreasing the drag reduction. At the same time, the integrated skin friction drag over the boat tail caused by the exhaust plume is diminishing as well. Moreover, the best theoretical

position of a BLI propulsor is at the trailing edge, since the entire momentum deficit in the boundary layer can be ingested.

The design parameters that describe the shaping of the nacelle appear to be of lesser importance. As discussed previously, the gradients for the parameters describing the aerodynamic shape of the nacelle are one or two orders of magnitude lower as compared to the other parameters. This is because the shape of the nacelle influence mostly the local drag production and have limited effect on the main flow field. Therefore, the optimization of the nacelle shape is most meaningful when the main design parameters have been fixed, provided that a feasible baseline nacelle geometry is provided.

The aforementioned trends and sensitivities are useful to perform design trade-off studies in the early design phase. Nevertheless, it should be kept in mind that the sensitivities could change if multiple design parameter are changed simultaneously. Furthermore, the presented trends are valid only for the baseline design. It is expected that the direction of the trends will remain similar for different designs, but the gradients and locations of apparent optima will shift, as these are design specific.

B. Optimization

Although the 1D sensitivities, discussed in the previous Section, are very useful for gaining an understanding of the design, it remains a challenging task to optimize the bare PFC by manual iteration. Therefore it is attempted to find the optimal design vector for the bare PFC using surrogate model gradient-based optimization. In the end, the optimized design will be compared to a previous bare PFC design.

1. Reduced design vector

To reduce the complexity of the optimization problem and enhance the fit of the surrogate model, the number of design variables could be reduced. However, elimination of design variables from the design vector will impact the accuracy of the model. A much reduced design vector could fail to capture the true global optimum. Depending on the quality and size of the sampling and the choice of surrogate model, the workable number of design variables that can be used is generally between 5-10 variables. Only the design variables that have a significant impact on the overall aerodynamic performance of the bare PFC are selected. This includes the FPR, duct height h_{duct} nozzle area ratio A_{18}/A_{12}, axial fan location x_{FF} and hub-to-tip-ratio $r_{\text{hub}}/r_{\text{tip}}$. Therefore, the reduced design vector becomes:

$$X = [\Pi, M, \text{FL}, h_{\text{duct}}, (A_{18}/A_2), (r_{\text{hub}}/r_{\text{tip}}), (x_{\text{FF}}/L)] \tag{4}$$

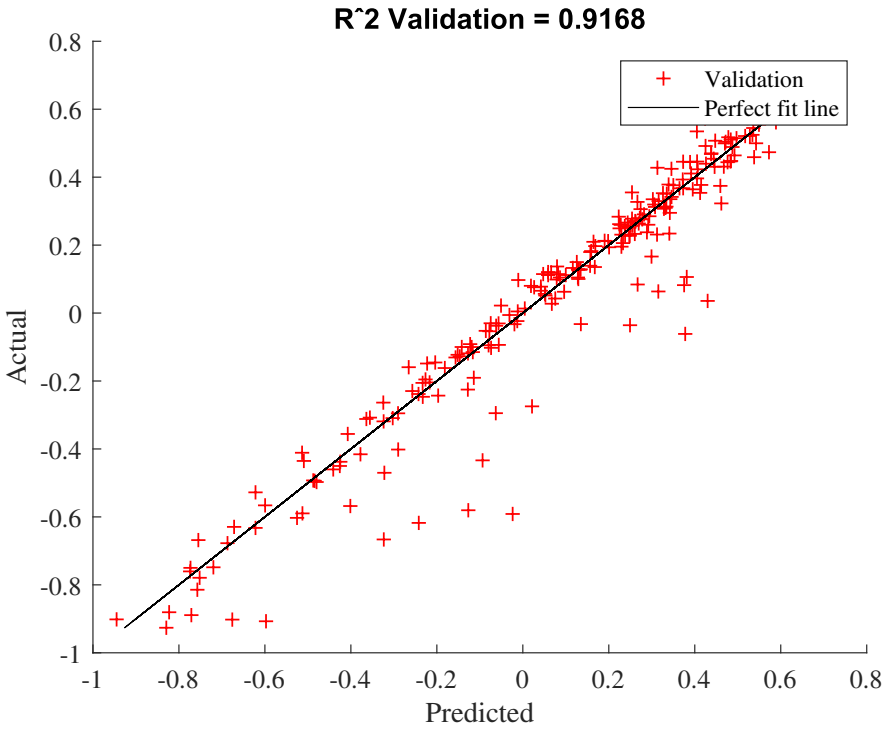

Fig. 10 Plot of predictions of $f_{\eta,PFC,bare}$ by the surrogate model and actual validation data

2. Surrogate model

Many different methods and models are in existence for application to aerodynamic optimization and design space exploration engineering problems [23]. Of the various methods under consideration, the Support Vector Regression (SVR) [34] was selected to be used in the optimization. The principle of SVR is to fit a kernel function with an acceptable error margin (ϵ) and tolerance (C) to the data. Optimization of the aforementioned hyper parameters ensures that the mean absolute error of the regression curve with respect to the data is minimized. For multi-dimensional data, the parameters ϵ and C are tuned to ensure an optimal fit of a hyper-surface to the data. In order to implement the method in the Matlab® framework, the software library LIBSVM [35] was used. Before fitting the data, the data was standardized to avoid numerical bias. To validate whether the fit of the model is good enough, a new set of samples was evaluated in the CFD framework. The samples were again generated using LPSS and distributed over the design space. In total 625 samples were generated, which resulted in 221 additional converged CFD results. The ϵ-SVR algorithm with a Radial Basis Function (RBF) kernel is used, as this resulted in the best fit of the model to the data. The quality of the fit of the surrogate model with the validation data is shown in Figure 10.

As can be observed, the fit is acceptable, with a coefficient of determination $R^2 = 0.9168$. In general the points of positive response ($f_{\eta,PFC,bare}$) are represented to a good extent by the surrogate model, with a few exceptions of

outliers. In the negative domain of the response, the validation data is sparser and the variation in the predictions with respect to the actual values is larger. This means that the model could give a reasonable fit for most combinations of parameters, but could also significantly under- or over-predict the response. To see how well the model is capable of capturing the trends, the model is verified with the 1D sensitivity data. The comparison is shown in Figure 11. As can be observed, the fit is reasonable in case the change in the response is large, such as is the case for the FPR for example. In case that the parameter is less sensitive, the error of the fit becomes too significant to provide an accurate prediction. This can be observed to be the case for the altitude and the axial FF position. Despite the fact that the error of the fit is too large to predict the response in all cases with sufficient accuracy, the qualitative behaviour of the model is acceptable. Only towards the boundaries of the domain, the accuracy of the model predictions appears to be decreasing. However, in general, the model should be sufficient to fine-tune the main design parameters of the PFC.

In order to estimate the required power by the FF during the optimization, a separate model is required. The necessity stems from the fact that the maximum power by the FF needs to be set by a constraint, to avoid a design with a too large power requirement. The auxiliary model is trained for the following parameters:

$$P_{\text{shaft,id}} = f(\Pi, M, (r_{\text{hub}}/r_{\text{tip}}), h_{\text{duct}}, (A_{18}/A_2)) \tag{5}$$

The model with 5 parameters is again fitted with the ϵ-SVR model with a RBF kernel. The data is compared with the same verification data set as used for the main surrogate model. Shown in Figure 12 is the validation plot, presenting the predictions of the model against the validation data. The coefficient of determination is relatively good with $R^2 = 0.9609$. Especially in the lower power spectrum up to about 8.0 MW, the model appears to predict the required output power quite well. The increased level of scatter in the predictions towards the higher power regime should not pose a problem for the current objective. Although the number of parameters that are included in the model for $P_{\text{shaft,id}}$ is less than the model to fit $f_{\eta,\text{PFC,bare}}$, the model for ideal shaft power appears to have less scatter in the data. As such, the data suggest that the scatter of the $f_{\eta,\text{PFC,bare}}$ parameter is due to the interactions of the various design parameters and their combined effect on the drag. The non-linear behaviour of the drag, for example, due to flow separations or shock waves, make it more difficult to fit the surrogate model with sufficient accuracy.

3. Optimization formulation

To optimize the geometry of the bare PFC, a Matlab® gradient-based solver (*fmincon*) is used in conjunction with the aforementioned surrogate models for $f_{\eta,\text{PFC,bare}}$ and $P_{\text{shaft,id}}$. Multiple starting points for the optimization process are selected to enhance the chance of finding a true optimum bare PFC design. To enhance the chance of finding an optimal design, three of the most promising designs are selected from the cloud of design points. The objective function for the

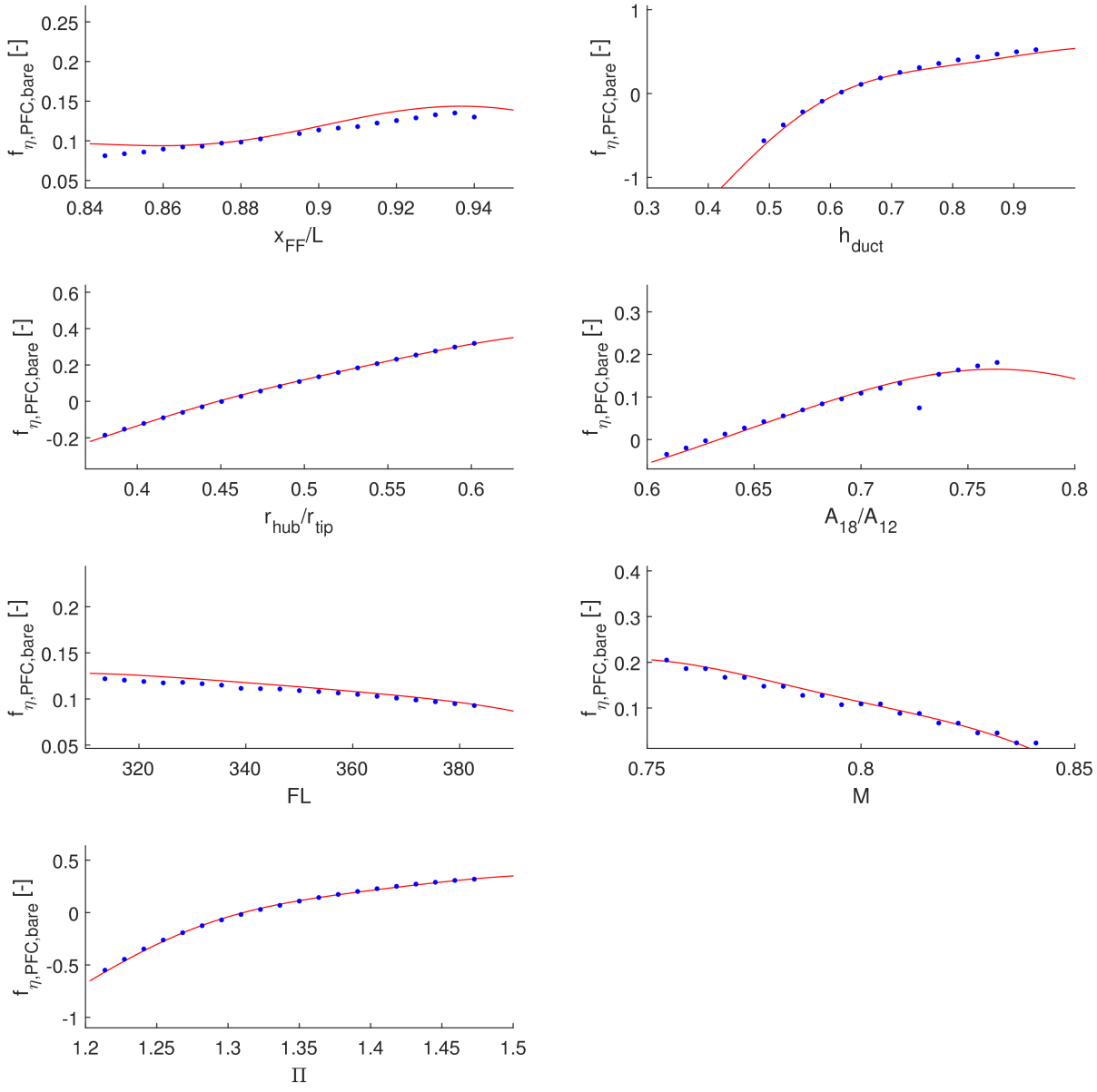

Fig. 11 Verification of surrogate model with 1-D sensitivity results obtained with CFD

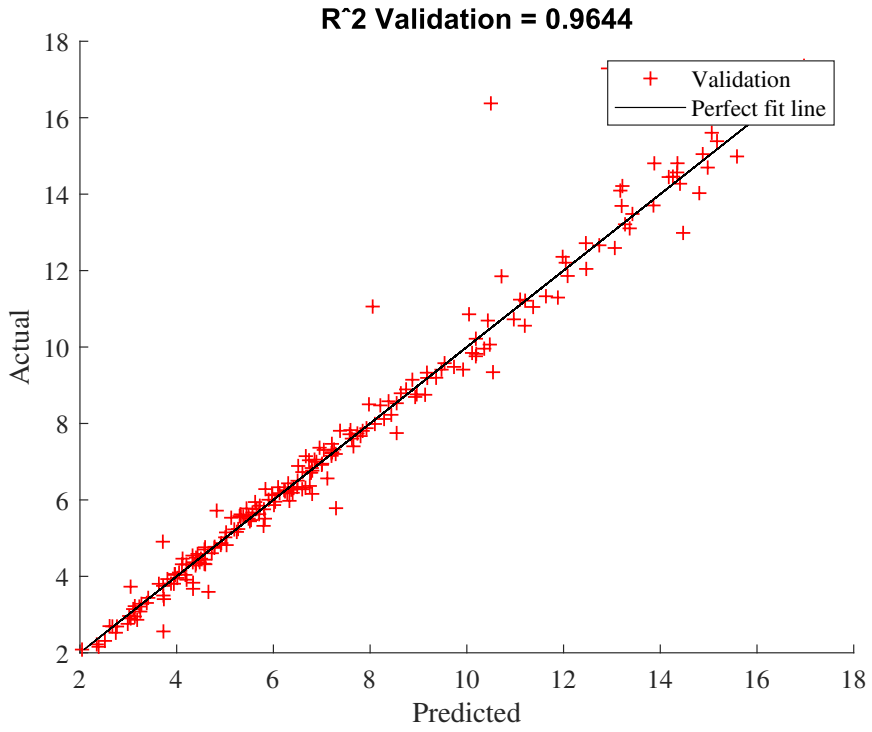

Fig. 12 Plot of predictions by the surrogate model for $P_{\text{shaft,id}}$ with actual validation data.

optimization is formulated as follows:

$$\text{Find:} \quad x^* = \arg\min f(x) = \frac{1}{f_{\eta,\text{PFC,bare}} + C} \tag{6}$$

In the above formulation, a constant is added to ensure that the objective value is always positive. To comply with the requirements for the PFC overall aircraft design [36] the optimization is constraint:

$$x_L < x < x_U \tag{7a}$$

$$FL - FL_{\text{ref}} = 0 \tag{7b}$$

$$M - M_{\text{ref}} = 0 \tag{7c}$$

$$P_{\text{shaft, id}} - P_{\text{shaft,max}} \leq 0 \tag{7d}$$

$$L_{\text{fus}} - L_{\text{fus, max}} \leq= 0 \tag{7e}$$

The equality constraints enforce that the optimizer finds an optimum solution for the operational conditions of the reference mission (FL= 350, M= 0.82). Furthermore, the maximum ideal power for the FF is limited to 5.5 MW, as the turbo-electric power-train of the CENTRELINE configuration is designed for this power output during cruise. Finally, a constraint is placed on the maximum fuselage length, not to exceed $L_{\text{fus,max}} = 70$m.

4. Results and verification

As a starting point for the optimization process, the cloud of available CFD results was surveyed for promising designs. Within margins of the operational conditions and upper limit for the ideal shaft power, the best-performing designs were picked and analysed. After assessment of the designs by engineering judgement, the best performing designs were selected. An overview of the 3 initial design vectors and the optimization results is shown in Table 4.

Table 4 Result of optimization using the 7 parameter surrogate model. Note that the performance parameters for the optimized result is a prediction by the model, in contrast to the CFD result of the initial configuration.

Optimum No.	Design vector	$f_{\eta,\text{PFC,bare}}$	$P_{\text{shaft, id}}$
1	x_0 = [1.35 0.80 350 0.65 0.70 0.50 0.90]	0.1090	6.20
	x^* = [1.32 0.82 350 0.73 0.68 0.43 0.92]	0.0334	5.50
2	x_0 = [1.35 0.81 352 0.89 0.65 0.43 0.85]	0.2511	16.91
	x^* = [1.32 0.82 350 0.73 0.68 0.43 0.92]	0.0325	5.50
3	x_0 = [1.46 0.81 358 0.63 0.63 0.43 0.89]	0.3886	11.80
	x^* = [1.32 0.82 350 0.73 0.68 0.43 0.92]	0.0334	5.50

x_0 *initial design vector* x^* *optimum design vector*

As can be observed from Table 4, the optimization algorithm finds the same optimum for three different initial points. The obtained optimum features a positive NPF compared to the bare PFC while not exceeding the limit on the ideal shaft power, constrained to a maximum of 5.50 MW. Since the surrogate model only provides an estimation of the aerodynamic performance, the selected designs are analysed separately by CFD simulation. The results are shown in Table 5.

As can be observed, the results are not satisfactory, since the required power appears to be under-estimated while the $f_{\eta,\text{PFC,bare}}$ is over-predicted. Moreover, the influence of the other design parameters, which are excluded from the surrogate model, can still have a significant impact on the aerodynamic performance. Nevertheless, the prediction for the second candidate design is within a 10% error margin, which is acceptable for initial design. Regardless of the quality of the fit, it can be observed from Table 5 that the 3rd candidate design has the best aerodynamic performance out of the three candidate designs. The $f_{\eta,\text{PFC,bare}}$ is positive, at the cost of a power requirement by the FF that is higher than what is considered to be the maximum power for the FF. By fine-tuning of the design parameters, the most

Table 5 Verification of prediction of the surrogate model for three different candidate designs with CFD results.

Optimum no.	Surrogate model		RANS CFD	
	$f_{\eta,\text{BLI}}$	$P_{\text{shaft,id}}$	$f_{\eta,\text{PFC,bare}}$	$P_{\text{shaft,id}}$
1	0.0334	5.50	0.0028	6.13
2	0.0325	5.50	0.0278	5.90
3	0.0334	5.50	0.0416	6.03

Table 6 Effect of successive design changes to the optimized design on $f_{\eta,\text{PFC,bare}}$ and $P_{\text{shaft,id}}$

Iteration No.	Description	$f_{\eta,\text{PFC,bare}}$ $[-]$	$P_{\text{shaft,id}}$ $[MW]$	$\Delta P_{\text{shaft,id}}$ [%]
0	Optimized design with $\Pi = 1.30$	-0.0365	5.52	-
1	As above with $\kappa_{\text{aft}} = 1.20$	-0.0339	5.51	-0.2%
2	As above with $\lambda_{\text{aft}} = 4.50$	-0.0281	5.50	-0.5%
3	As above with $D_{\text{fus}} = 5.80$	-0.0273	5.47	-0.9%

promising candidate design can be improved further and made compliant with the constraints. Since the ideal shaft power is very sensitive to the changes in FPR, the FPR is reduced slightly to bring down the required shaft power for the third design. This comes at the cost of the NPF, which just becomes negative. With the knowledge gained from the sensitivity analysis, one can adjust some of the other design parameters, which have not been taken into account in the optimization. For example, the slenderness of the aft section can be reduced while the shape of the aft section is made more convex. Similarly, the fuselage diameter is reduced effectively increasing the Fuselage Slenderness Ratio. The effect of the successive design changes is shown in Table 6.

As can be seen in the table above, the changes have been effective in increasing the $f_{\eta,\text{PFC,bare}}$. Equally important, the ideal shaft power $P_{\text{shaft,id}}$ of the FF was reduced by almost 1%. At the same time the BLI efficiency factor was improved. A comparison of the PFC geometry before and after the aforementioned modifications is shown in Figure 13. As can be seen, the modified design features a slightly shorter fuselage as a result of the reduced fuselage diameter. Furthermore, the curvature of the aft body is more convex, resulting in a steeper curvature of the aft-body ahead of the FF. The latter means that the boundary layer is facing a steeper adverse pressure gradient. Despite the small increase of the wetted surface area, the drag is found to be reduced by $\Delta D_{\text{PFC,bare}} = -0.7$%.

To understand the aerodynamic behaviour of the improved PFC design better, the contour plots of the Mach number and total pressure (Figure 15) are included. As can be observed from the Mach number contours, the flow field does not show any regions of separated flow or shock waves. The flow over the nacelle remains subsonic, an indication that there is no excessive spillage drag. At the duct exit, the flow is expanded to atmospheric conditions. Due to the curvature at the start of the boat-tail, the flow is locally accelerated. Inspection of the total pressure contours shows that the FF ingests a majority of the momentum deficit of the fuselage boundary layer. The momentum added to the flow by the FF is more than what is required for just filling the wake, as was found to be necessary to offset the additional drag of the nacelle.

C. Comparison with reference design

Having achieved an improved design, it is interesting to compare the new design with the previous (Rev05) PFC design within the CENTRELINE project. The latter was obtained by subsequent manual design iterations based on

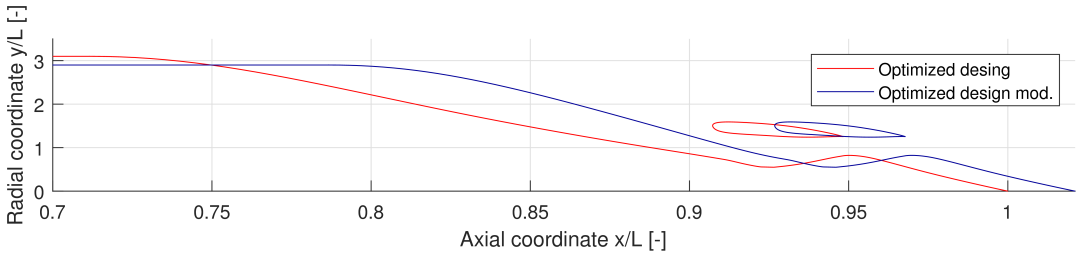

Fig. 13 Comparison of inital optimized bare PFC geometry and subsequent modified design of the PFC

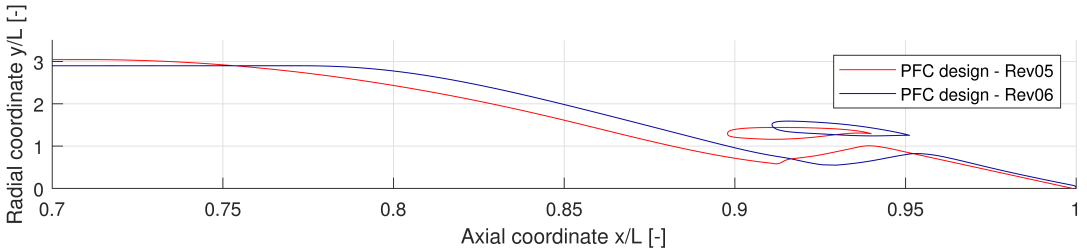

Fig. 14 Comparison of the geometry of the Rev06 design with the previous (Rev05) PFC design

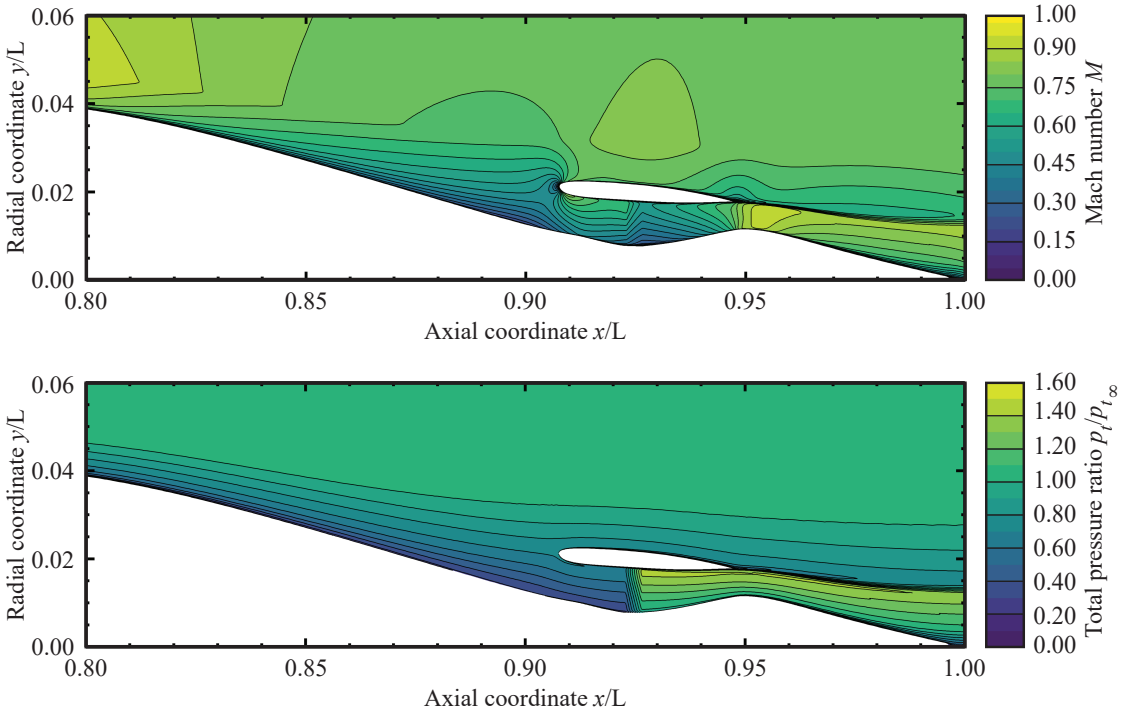

Fig. 15 Contours of normalized Mach number (top) and total pressure (bottom) for the Rev06 PFC geometry (M=0.82, FL=350, ISA +10 K)

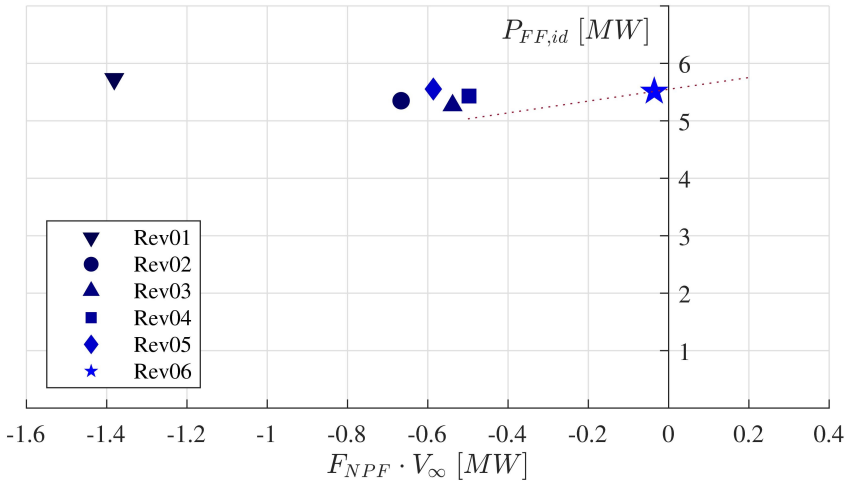

Fig. 16 Comparison of the Fuselage Fan idealized power versus the F_{NPF} times flight velocity for the improved design with previous revisions of the PFC design. (M=0.82, FL=350, ISA + 10 K) [37]

engineering judgement. Note that the Rev05 PFC design features a design FPR= 1.40 [16]. Shown in Figure 16 is the FF shaft power versus the product of the NPF and flight velocity. As can be observed, the improved design (called Rev06) is a significant improvement in terms of $f_{\eta,\text{PFC,bare}}$ over the previous revisions of the PFC design. Even though the NPF is still negative at this given power, the difference in the net balance of the propulsive force and the drag is $\Delta F_{\text{NPF}} \approx 1.50kN$. This corresponds to about 4% of the bare (i.e. no wings and empennage) PFC drag. A study on the aircraft level should be conducted to evaluate how much the relative reduction of total net force of the complete aircraft is and how the total system efficiency is affected. At the current design point, the FPR= 1.30, which is on the lower side of the spectrum. Further increasing the FPR is beneficial for the aerodynamic performance, as found already by the data presented in Figure 9. However , this would require an increased power output by the hybrid-electric drivetrain, adding additional weight and cooling complexity. To compare Rev05 and Rev06 directly, one should evaluate both designs for equal level of F_{NPF}. In case the FPR of Rev06 is lowered such that it matches the F_{NPF} of Rev05, it can be shown that the Rev06 design requires close to $\Delta P_{\text{shaft,id}} \approx 10\%$ less power. This is shown graphically by the dotted line in 16. The latter was obtained from a curve-fit from RANS CFD simulations for the optimized design with varying values for FPR.

To see how the design is actually different from the previous PFC design (Rev05), the geometries are compared with each other. This is presented in Figure 14. As can be observed the fuselage length of both designs is comparable, despite the fact that the fuselage diameter of the Rev06 design is lower. However, this is compensated for by the increased internal volume in the aft section, which is less slender and has a more convex shaping of the fuselage contour. Furthermore, it can be seen that the incidence angle of the nacelle is much larger for the Rev06 design, compared to the Rev05 PFC geometry. Although both nacelles are approximately equal in size, the duct height of the Rev06 is higher due to the

lower hub-to-tip ratio. The minimum radius at the hub is $r_{\text{hub}} = 0.56$m, which is sufficient space to allocate the electric motor [38].

V. Conclusion

The Propulsive Fuselage Concept (PFC) is a tube-and-wing aircraft architecture which uses an additional propulsor, integrated in the aft-cone of the fuselage, to maximize the aerodynamic efficiency by exploiting Boundary Layer Ingestion (BLI). To understand and maximize the aerodynamic performance of the PFC, a systematic survey of the aerodynamic design space has been performed. A methodology based on the novel Design of Experiments techniques has been implemented. The methodology comprises of the following elements:

1) A parametric model has been constructed to describe the geometry of the bare PFC (i.e. fuselage body with integrated BLI propulsor). In total 23 design variables were used for the representation of the geometry, including the aerodynamic shape of the nacelle.
2) A quasi-random sampling strategy was employed to span the entire aerodynamic design space. In total $9,600$ samples were used as input for CFD frame-work. Approximately one-third of the samples resulted in a converged CFD simulation
3) The development of a fully automated CFD pre- and post-processing MATLAB® framework has enabled the analysis of several thousand unique samples of the design vector using CFD simulations.
4) Axisymmetric 2D RANS simulations were performed for the aerodynamic analysis of the PFC, representing the best compromise between fidelity of the modelled flow field and computational effort. A simple body-force model was implemented to model the BLI propulsor. The propulsor model was robust and did not compromise the computational cost. Moreover, it allowed for a direct control of the imposed FPR and an effective calculation of the propulsive force and power.
5) In order to enhance the physical understanding of the aerodynamics of the PFC, a one-dimensional sensitivity study has been conducted to map the relative influence of each individual design parameter on the aerodynamic performance of the PFC.
6) A surrogate model using a reduced number of design variables was constructed and successfully verified. Of the initial 26 design variables, 7 of the most influential parameters, as selected through the sensitivity analysis, were used to construct the surrogate model.
7) A gradient-based optimization with the reduced design parameters was performed to find an optimum set of parameters. By selection of the most promising designs of the data set and application of the optimization results, a local optimum design was found The objective function was the so-called BLI efficiency factor, defined as $f_{\eta,\text{PFC,bare}} = F_{\text{NPF}} \cdot V_{\text{inf}} / P_{\text{shaft,id}}$. This scalar parameter represents a measure of the useful work done by the Net

Propulsive Force (NPF) and the idealized shaft power.

Verification of the aerodynamic performance in RANS CFD showed that the prediction of the surrogate model was satisfactory, despite an apparent offset of the prediction compared to the CFD data. Successive adjustment of the non-optimized design parameters, on the basis of the sensitivity study, further improved the aerodynamic performance of the design. The optimized design, compared to previous PFC designs, features:

- Increased duct height h_{duct}
- Reduced Fan Pressure Ratio (FPR) from $\Pi = 1.40$ to $\Pi = 1.30$
- 10% reduction in ideal shaft power $P_{FF,id}$ at equal net force

The increased height of the duct of the Fuselage Fan (FF) ensures that a larger portion of the momentum deficit of the boundary layer is ingested by the FF. To account for the increased mass-flow in the duct, the FPR of the fan is reduced to meet the imposed limit on the ideal shaft power by the FF. Other modifications include an increased incidence angle of the nacelle for better alignment with the incoming flow and reduced fuselage diameter. At a similar NPF, the improved design would require approximately 10% less power, which is a significant improvement. CFD analysis of the improved design shows that the aerodynamic design is feasible, without any signs of major flow defects. Both the initial and optimized design increase the momentum and energy in the wake than would be required for pure wake-filling design.

Although a full optimization resulting in a global optimum has not been the outcome of the current study, the methodology applied has been successful to make a significant improvement to the aerodynamic design. Moreover, further insight has been gained into the sensitivity of the design parameters to the aerodynamic performance of the PFC.

Acknowledgements

This work was conducted within the CENTRELINE project, which has received funding from the European Union's Horizon 2020 research and innovation programme under Grant Agreement No. 723242. The authors would like to thank Dr. M. Pini for the discussions about Design of Experiments (DoE) and surrogate modelling.

References

[1] *Flightpath 2050: Europe's Vision for Aviation*, ACARE, 2011.

[2] *Strategic Research and Innovation Agenda*, ACARE, 2011.

[3] Beck, N., Landa, T., Seitz, A., Boermans, L., and Y. Liu, R. R., "Drag Reduction by Laminar Flow Control," *Energies*, Vol. 11, No. 1, 2018.

[4] Pornet, C., and A.T.Isikveren, "Conceptual design of hybrid-electric transport aircraft," *Progress in Aerospace Sciences*, Vol. 79, 2015, pp. 114–135.

[5] Drela, M., "Power Balance in Aerodyanmic Flows," *AIAA Journal*, Vol. 47, No. 7, 2009.

[6] Peijian, L., Ragni, D., Hartuc, T., and Veldhuis, L., "Experimental Investigation of the Flow Mechanisms Associated with a Wake-Ingesting Propulsor," *AIAA Journal*, Vol. 55, No. 4, 2016.

[7] Steiner, H., Seitz, A., Wieczorek, K., and Plotner, K., "Multi-Disciplinary Design and Feasibility Study of Distributed Propulsion Systems," *28th International Congress of the Aeronautical Sciences*, edited by ICAS, 2012.

[8] Isikveren, A., Seitz, A., Bijewitz, J., Hornung, M., Mirzoyan, A., and Isyanov, A., "Recent Advances in Airframe-Propulsion Concepts withDistributed Propulsion," *29th International Congress of the Aeronautical Sciences*, edited by ICAS, 2014.

[9] Welstead, J., and Felder, J., "Conceptual Design of a Single-Aisle Turbo-electric Commercial Transport with Fuselage Boundary Layer Ingestion," *54th AIAA Aerospace Sciences Meeting*, edited by Sci-Tech, 2016.

[10] Gray, J., and Martins, J., "Coupled Aeropropulsive Design Optimization of a Boundary Layer Ingestion Propulsor," *The Aeronautical Journal*, Vol. 123, No. 1259, 2019, pp. 121–137.

[11] Kenway, G., and Kiris, C., "Aerodynamic Shape Optimization of the STARC-ABL Concept for Minimal Inlet Distortion," *Structures, Structural Dynamics and Materials Conference*, edited by Sci-Tech, 2018.

[12] Ordaz, I., Nielsen, E., and Rallabhandi, S., "Adjoint-Based Design of a Distributed Propulsion Concept with a Power Objective," *AIAA Aviation Forum*, edited by AIAA, 2019.

[13] Yildrim, A., J., G., Mader, C., and Martins, J., "Aeropropulsive Design Optimization of a Boundary Layer Ingestion System," *AIAA AVIATION Forum,*, edited by AIAA, 2019.

[14] Hahn, A., "Vehicle Sketch Pad: A Parametric Geometry Modeler for Conceptual Aircraft Design," *48th AIAA Aerospace Sciences Meeting Including the New Horizons Forum and Aerospace Exposition*, edited by AIAA, 2010.

[15] Brown, K., Fleming, J., Langford, M., and Ng, W., "Development of a Ducted Propulsor for BLI Electric Regional Aircraft - Part I: Aerodynamic Design and Analysis," *AIAA Propulsion and Energy 2019 Forum*, edited by AIAA, 2019.

[16] Seitz, A., Peter, F., Bijewitz, J., Habermann, A., Goraj, Z., Kowalski, M., Pardo, A. C., Hall, C., Meller, F., Merkler, R., Petit, O., Samuelsson, S., Corte, B. D., van Sluis, M., Wortmann, G., and Dietz, M., "Concept Validation Study for Fuselage Wake-Filling Propulsion Integration," *31st Congress the International Council of the Aeronautical Sciences*, edited by ICAS, 2018.

[17] CENTRELINE, "Project Public Website," `http://www.centreline.eu`, 2020.

[18] Seitz, A., Habermann, A., Peter, F., F.Troeltsch, Pardo, A. C., Corte, B. D., van Sluis, M., Goraj, Z., Kowalski, M., Zhao, X., Grönstedt, T., Bijewitz, J., and Wortmann, G., "Proof of Concept Study for Fuselage Boundary Layer Ingesting Propulsion," *Aerospace*, Vol. 8, 2021.

[19] Chappell, P. D., Clarke, A., Porter, R., and Wood, S., *ESDU 77028: Geometrical characteristics of typical bodies*, ESDU, November 1977.

[20] Peter, F., Bijewitz, J., Habermann, A., Ludemann, M., Plotner, K., Seitz, A., and Troelsch, F., "Definition of the CENTRELINE reference aircraft and power plant systems," *69th Deutscher Luft- und Raumfahrtkongress (DLRKs)*, edited by D. G. für Luft-und Raumfahrt (DGLR), 2020.

[21] Piegl, L., "On NURBS: A Survey," *IEEE Computer Graphics and Applications*, Vol. 11, 1991.

[22] Derksen, R., and Rogalsky, T., "Optimum Airfoil Parameterization for Aerodynamic Design," *Computer Aided Optimum Design in Engineering*, Vol. 106, 2009.

[23] Yondo, R., Andres, E., and Valero, E., "A review on design Of Experiments and Surrogate Models in Real-Time and many-query Aerodynamic Analysis," *Progress in Aerospace Science*, Vol. 96, 2018.

[24] Shields, M., and Zhang, J., "The Generalization of Latin Hypercube Sampling," *Reliability Engineering and System Safety*, Vol. 148, 2016.

[25] Hofer, D., "Matlab to Ansys ICEM/Fluent and Spline Drawing Toolbox," , July 2019. URL `https://www.mathworks.com/matlabcentral/fileexchange/66215-matlab-to-ansys-icem-fluent-and-spline-drawing-toolbox`.

[26] Sutherland, W., "The viscosity of gases and molecular force," *Philosophical Magazine Series 5*, Vol. 36:223, 1893.

[27] Menter, F., "Two-Equation Eddy-Viscosity Turbulence Models for Engineering Applications," *AIAA Journal*, Vol. 32, 1994, p. 1598–1605.

[28] Leonard, B., "A stable and accurate convective modelling procedure based on quadratic upstream interpolation," *Computer Methods in Applied Mechanics and Engineering*, Vol. 19, 1979, p. 59–98.

[29] van Leer, B., "Towards the Ultimate Conservative Difference Scheme, V. A Second-Order Sequel to Godunov's Method," *Journal of Computational Physics*, Vol. 32, 1979, p. 101–136.

[30] Pardo, A. C., and Hall, C., "Aerodynamics of boundary layer ingesting fuselage fans," *ASME Journal of Turbomachinery*, Vol. 143, 2021.

[31] Habermann, A., Zahn, R., Seitz, A., and Hornung, M., "Multidimensional Parametric Study of a Propulsive Fuselage Concept Using OpenFOAM," *AIAA AVIATION 2020 (virtual conference)*, edited by AIAA, 2020.

[32] Pearson, K., "On Lines and Planes of Closet Fit to Systems of Points in Space," *Philosophical Magazine*, Vol. 11, 1901, pp. 559–572.

[33] Berguin, S., "A Method for Reducing Dimensionality in Large Design Problems with Computationally Expensive Analysis," Ph.D. thesis, Georgia Institute of Technology, http://hdl.handle.net/1853/53504, 2 2015.

[34] Awad, M., and Khanna, R., "Support Vector Regression," *Efficient Learning Machines: Theories, Concepts, and Applications for Engineers and System Designers*, Apres, 2015, pp. 67–80.

[35] Chang, C., and Lin, C., "LIBSVM: a Library for Support Vector Machiness," *ACM Transactions on Intelligent Systems and Technology*, Vol. 2, 2011, pp. 1–27. Software available at `http://www.csie.ntu.edu.tw/~cjlin/libsvm`,.

[36] Habermann, A., Troelsch, F., Peter, F., Maas, P., van Sluis, M., Kowalski, M., Wortmann, G., Bijewitz, J., and Seitz, A., "Summary Report on Multi-Disciplinary Design Results," Tech. Rep. CENTRELINE Project Deliverable D2.11, Bauhaus Luftfart, November 2020.

[37] Seitz, A., Habermann, A., and van Sluis, M., "Optimality considerations for propulsive fuselage power savings," *Proceedings of the Institution of Mechanical Engineers, Part G: Journal of Aerospace Engineering*, Vol. 235, 2021.

[38] Wortmann, G., "Electric Machinery Preliminary Design Report," Tech. Rep. CENTRELINE Project Deliverable D4.04, SIEMENS, October 2018.